Modeling Solid-Fuel Ramjet Combustion

David W. Netzer*
Naval Postgraduate School, Monterey, Calif.

A computer model was developed for the solid-fuel ramjet combustor. The model appears to be a good qualitative tool for examining the effects of combustor geometry and test environment on fuel regression rate, flame pattern, and combustion efficiency. Additional model verification is required.

Nomenclature

B = mass transfer parameter, $(h_p - h_0)/(h_0 - h_T)$
C_1, C_2 = coefficients in k-ϵ turbulence model
C_P = specific heat at constant pressure
C_{f0} = friction coefficient without mass addition
G = generation term in equations for k and ϵ,

$$\mu_{\text{eff}}\left\{2\left[\left(\frac{\partial V_z}{\partial z}\right)^2+\left(\frac{\partial V_r}{\partial r}\right)^2+\left(\frac{V_r}{r}\right)^2\right]+\left(\frac{\partial V_z}{\partial r}+\frac{\partial V_r}{\partial z}\right)^2\right\}$$

G_{air} = mass flux of air based on bulk velocity
h = enthalpy, $C_P(T-T^0)+m_{\text{ox}}H_0/i$
H_0 = effective heat of combustion, cal/g of fuel
i = stoichiometric ratio of oxygen mass to fuel mass
k = turbulence kinetic energy
l_p = "length scale" of eddies at near-wall grid point P
m = mass fraction
$\dot{m}''$ = mass flux from fuel surface
$\bar{M}$ = average molecular weight
p = pressure
P_r = molecular Prandtl number
r = radial coordinate
$\dot{r}$ = regression rate of fuel surface
R = universal gas constant
R_e = near-wall grid Reynolds number, $\bar{\rho}\bar{V}y_p/\mu_0$
R_t = turbulent Reynolds number, $k_P^{1/2}y_P\rho/\mu_0$
S_ϕ = source term in differential equation for generalized dependent variable ϕ
T = temperature
V = velocity
y_P = distance from wall to near-wall grid point P
y_P^+ = nondimensionalized distance from wall, $(\rho/\mu_0)(\tau_0/\rho)^{1/2}y_P$
z = axial coordinate
γ = slip function from Couette flow for boundary condition on k
ϵ = rate of dissipation of turbulence energy
μ = molecular viscosity
μ_{eff} = turbulent viscosity
ρ = density
σ_{eff} = effective turbulent Prandtl or Schmidt number
τ = shear stress
ϕ = generalized dependent variable
ψ = streamfunction
ω = vorticity

Subscripts

fu = fuel
h = enthalpy
N_2 = nitrogen
$0,w$ = wall
of = refers to the "property" $m_{\text{fu}} - m_{\text{ox}}/i$
ox = oxygen
P = near-wall grid point
r = radial component
T = reference condition deep within fuel grain
z = axial component
θ = tangential component

Superscripts

0 = reference conditions
$\bar{\ }$ = average value

Received May 26, 1977; revision received Aug. 15, 1977.
Index categories: Airbreathing Propulsion; Combustion and Combustor Designs; Computational Methods.

*Associate Professor, Department of Aeronautics. Member AIAA.

Introduction

THE solid-fuel ramjet (SFRJ) may utilize a sudden dump inlet for flame stabilization and some means of mixing downstream of the fuel grain in order to burn all of the available fuel that is in the gas phase (Fig. 1). Experimental data[1] have shown that the recirculation zone is fuel rich and that the primary combustion region (or flame zone) spreads out from along the shear layer between the recirculation zone and the inlet flow. The flame has been observed to be quite broad near the flow reattachment position and subsequently develops into a turbulent diffusion flame within the developing boundary layer downstream of reattachment. In order to guide development efforts and to provide needed input to systems analysis studies, combustion models are needed which can predict the fuel regression rate, flammability limits, and combustion efficiency as a function of hardware design and operating environment. Previous work[2] has been directed toward adaptation of the Gosman et al. PISTEP II model[3,4] for heat and mass transfer in recirculating flows to the SFRJ geometry. That work considered the effects of finite rate kinetics and combustor geometry on the flame pattern and internal flowfield.

Several weaknesses were evident in the earlier work. Fuel regression rates were not calculated. Also, the flame pattern was not in agreement with experimental data; i.e., the recirculation region was predicted to be oxidizer rich, and the flame within the boundary-layer region spread too rapidly toward the centerline of the motor. In addition, the model had not been adequately checked for accuracy against experimental data for velocity, pressure, and turbulence intensity. The present investigation was conducted to improve the qualitative accuracy of the model, to incorporate prediction of the fuel regression rate, and to check the validity of the model against experimental data.

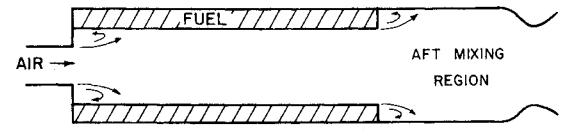

Fig. 1 Schematic of solid-fuel ramjet.

Model Overview

The basic assumptions were that the flow was steady, recirculating, two-dimensional, and subsonic. In addition, kinetic heating and vorticity sources resulting from spatial gradients in the effective viscosity were neglected. The turbulent Lewis number was taken to be unity. The transformed variables of vorticity ω/r and streamfunction ψ were used, together with enthalpy h and species mass fractions (oxidizer, fuel, etc.). A modified Jones-Launder[4-6] two-equation turbulence model was used to calculate the viscosity throughout the flowfield. Thus, two additional variables must be considered, the turbulence kinetic energy k and the turbulence energy dissipation rate ϵ. The modified Jones-Launder model incorporates five empirical constants, and the effective viscosity is calculated using the following expression:

$$\mu_{\text{eff}} = 0.09\rho k^2/\epsilon \tag{1}$$

In the present study, the combustion was considered to be mixing limited with a one-step simple chemical reaction. Thus, 1 g fuel $+ i$ g oxidizer $\rightarrow (1+i)$ g of products, and fuel and oxidizer could not exist together. Species considered were oxygen, nitrogen, fuel, and products. The present form of the model neglected radiation, and density was calculated using $\rho = p\bar{M}/RT$.

With these assumptions, the governing equations for axisymmetric flow can be cast in the standard elliptic format[3-5]:

$$\underbrace{a_\phi\left[\frac{\partial}{\partial z}\left(\phi\frac{\partial\psi}{\partial r}\right)-\frac{\partial}{\partial r}\left(\phi\frac{\partial\psi}{\partial z}\right)\right]}_{\text{convection terms}} \underbrace{-\frac{\partial}{\partial z}\left[b_\phi r\frac{\partial(C_\phi\phi)}{\partial z}\right]-\frac{\partial}{\partial r}\left[b_\phi r\frac{\partial(C_\phi\phi)}{\partial r}\right]}_{\text{diffusion terms}} + \underbrace{rS_\phi}_{\text{source term}} = 0 \tag{2}$$

where the parameters are presented in Table 1. Additional discussion of these equations and utilization of various turbulence models can be found in Refs. 7 and 8.

Boundary Conditions and Solution Procedure

The inlet flow was considered to be "plug flow," although other inlet conditions (distortion, etc.) are easily incorporated. The inlet turbulence intensity was taken to be 5.2% in order to closely match experimental measurements. Axial gradients for all variables were considered zero at the flow exit and were taken as zero for all "conserved properties" ($m_{\text{fu}} - m_{\text{ox}}/i$, m_{N_2}, h) at the step-face. Radial gradients for all variables except ψ were taken as zero at the axis of symmetry. The major area of concern in the specification of boundary conditions for the SFRJ is along the fuel surface. When calculations are made with the model for an adiabatic or isothermal wall with no mass addition, inaccuracies in the turbulence model are somewhat masked. The fuel mass addition at the wall and the subsequent combustion greatly amplify the need for accurate effective viscosity calculations near the wall if observed experimental behavior is to be approximated.

All "conserved" properties, when in dimensionless form, had identical governing equations and boundary conditions. Thus, only one equation was required to be solved for all "conserved" properties. The resulting set of five equations (ω/r, ψ, k, ϵ, $m_{\text{fu}} - m_{\text{ox}}/i$) was cast in finite-difference form and solved using the Gauss-Seidel method with upwind differences and relaxation. Under relaxation was required: 0.5 for ω/r and ψ, 0.3 for k and ϵ, and 0.9 for $m_{\text{fu}} - m_{\text{ox}}/i$. A nonuniformly spaced 17×25 rectangular grid system was employed. Solution was performed on an IBM 360-67 using Fortran H and required approximately 35 min to complete 1000 iterations.

The fuel surface was considered to have a uniform and constant temperature, and the mass fraction of oxidizer at the surface was considered to be zero. In order to obtain a fuel-rich recirculation zone, a boundary-layer flame pattern in agreement with experiment, and accurate conservation of species, several modifications had to be made to the original model.[4,6] For simplicity, the boundary layer was considered to consist of two parts, a laminar sublayer and a turbulent layer. The border between the two regions was considered to occur where $y_p^+ = 24$. At each near-wall grid point, y_p^+ was calculated:

$$\text{if } y_p^+ > 24: \quad C_{f0}/2 = 0.02846/R_e^{0.25} \tag{3}$$

The velocity profile was corrected for blowing,[9] and μ_{eff} was calculated using Eq. (1):

$$\text{if } y_p^+ \le 24: \quad C_{f0}/2 = 2/R_e \tag{4}$$

The laminar viscosity was calculated using

$$\mu = \mu_0 (T/T_0)^{0.5} \tag{5}$$

In the actual calculation procedure, the grid was selected to insure that $y_p^+ \le 24$. The value of 0.02846 is required for matching of the two-zone boundary layer.

The boundary condition for vorticity was calculated from

$$(\omega/r)_0 = \tau_0/\mu_0 r_w \tag{6}$$

where $\tau_0 = (C_{f0}/2)\bar{\rho}\bar{V}^2 \ell n\,(1+B)/B$, in which the wall shear stress is corrected for blowing by using the simple Couette flow approximation $\ell n(1+B)/B$. The control volumes used at the fuel surface for the microintegration are shown in Fig. 2. The control volumes for all variables but k and ϵ were taken to the wall. For k and ϵ, the control volumes were taken to the half-grid point. Gradients at the wall for "conserved" properties were taken to be of the form

$$\left(\frac{\partial h}{\partial y}\right)_0 = \left\{\frac{(h_p - h_0)}{yp}\right\}\frac{\ell n(1+B)}{B} \tag{7}$$

The wall mass flux provided the boundary condition for ψ and was calculated from

$$\dot{m}'' = \left(\frac{\mu_0}{p_r}\right)\left(\frac{\partial h}{\partial y}\right)_0 \Big/ (h_0 - h_T) = \left(\frac{\mu_0}{p_r}\right)\frac{\ell n(1+B)}{y_p} \tag{8}$$

The boundary condition on k was calculated from[4]

$$k_0 = \gamma k_p \tag{9}$$

where

$$\gamma = -1.0 \quad (R_t \le 19.8)$$

$$= -0.39 \quad (R_t > 19.8)$$

The boundary condition on ϵ was considered to occur at the near-wall grid point:

$$\epsilon_p = k_p^{3/2}/l_p \tag{10}$$

where

$$l_p = 0.2y_p \quad (y_p^+ < 24) \tag{11}$$

$$l_p = 0.4y_p \quad (y_p^+ > 24) \tag{12}$$

The boundary conditions for ω/r, k, and ϵ on the step-face were calculated in a similar manner except that there was no wall mass addition, none of the microintegration control volumes were extended to the wall, and $l_p = 2.44\, y_p$.

Launder and Spalding[10] have discussed the strengths and weaknesses of the k-ϵ model using both the wall function and low-Reynolds-number modeling methods. They indicate that modification of the boundary conditions on ϵ sometimes was found necessary on the step-face in order to obtain results in agreement with experiment. In this investigation, wall functions were employed for the k-ϵ model. Since the mass addition rates were low ($B<1.5$), the five constants in the model[4-6] were not modified. When $y_p^+ < 24$ along the fuel grain, the effective viscosities predicted using the k-ϵ model were not used at the near-wall grid points. In this case, the boundary conditions given by Eqs. (10-12) were required to provide realistic values of μ_{eff} and fuel mass fraction at the second grid point from the wall. An alternate procedure could have been to use the low-Reynolds-number modeling methods.[6,10] In recent work with smaller inlet step heights, it has been found necessary to employ Eqs. (10-12) for ϵ_p along the step-face. Much additional work is apparently required to better define the near-wall region.

The finite-difference equations[3,4] require the use of space-averaged values for the source terms presented in Table 1. At the near-wall grid points, large gradients exist if $y_p^+ > 24$. As mentioned previously, this was prevented at the fuel surface by appropriate selection of the radial grid spacing. Along the step-face, however, integrated average values had to be calculated for ω/r and all velocity gradients. Velocity profiles along the step-face for $y_p^+ > 24$ were assumed to obey the 1/7th power law. In order to obtain realistic solutions, the streamfunction at the grid point downstream of the step inlet was required to be held fixed at the value that existed at the step corner.

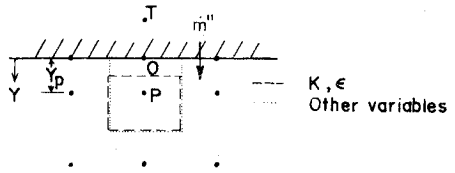

Fig. 2 Near-wall control volumes.

Results and Discussion

Divergence would occur in the iteration unless the initial conditions specified for ω/r and ψ were in close agreement (for example, 1/7th power-law distributions). It was also necessary to prescribe an initial length scale distribution. The length scale distribution was used to calculate initial values of ϵ from k using Eq. (10). The ϵ field was held constant for an initial 35 iterations in order to promote convergence. Specification of the initial length scale distribution required trial-and-error methods for other than the simple rearward-facing step geometry. Variations in gas density were also prevented from varying for the first 50 iterations.

At each axial location, species and energy conservation calculations were made. False diffusion errors were larger in the recirculation zone, where the grid lines were at large angles to the streamlines. Small errors in the solution of the "conserved" property equation presented some difficulties, since m_{fu}, m_{ox}, m_{pr}, and m_{N_2} were all calculated from the one solution. Calculation of fuel conservation was especially difficult, since fuel concentration gradients near the wall were very large. In general, energy and species (other than fuel) were conserved to within 5%. With these accuracies, fractional changes between iterations were a maximum of 0.3%. This required between 750 and 1000 iterations. The "conserved" properties and streamfunction converged more rapidly than did ω/r, k, and ϵ. For the higher inlet velocities,

Table 1 Equation parameters

ϕ	a_ϕ	b_ϕ	C_ϕ	S_ϕ
$\frac{\omega}{r}$	r^2	r^2	μ_{eff}	$-\frac{\partial}{\partial z}(\rho V_\theta^2) - r\left[\frac{\partial}{\partial z}\left(\frac{V_r^2+V_z^2}{2}\right)\frac{\partial \rho}{\partial r} - \frac{\partial}{\partial r}\left(\frac{V_r^2+V_z^2}{2}\right)\frac{\partial \rho}{\partial z}\right]$ $-r^2 S_\omega$
ψ	0	$\frac{1}{\rho r^2}$	1	$-\frac{\omega}{r}$
$m_{\text{fu}} - \frac{m_{\text{ox}}}{i}$	1	$\frac{\mu_{\text{eff}}}{\sigma_{of}}$	1	0
m_{N_2}	1	$\frac{\mu_{\text{eff}}}{\sigma_{\text{N}_2}}$	1	0
h	1	$\frac{\mu_{\text{eff}}}{\sigma_h}$	1	0
k	1	$\frac{\mu_{\text{eff}}}{\sigma_k}$	1	$-(G-\rho\epsilon)$
ϵ	1	$\frac{\mu_{\text{eff}}}{\sigma_\epsilon}$	1	$-(C_1 G\epsilon/k - C_2\rho\epsilon^2/k)$

$C_1 = 1.45$, $C_2 = 2.0$, $V_\theta = 0$
$S_\omega = S_\omega$ (gradients in μ_{eff}) — neglected[3,8]
$\sigma_h = \sigma_{of} = \sigma_{\text{N}_2} = 1.0$, $\sigma_\epsilon = 1.3$

the relaxation parameter for ω/r had to be reduced to values between 0.3 and 0.4.

The location of the "reattachment point" was found to be somewhat sensitive to the distance from the step-face to the first axial grid line. This resulted from specification of the streamfunction as unchanging, as discussed previously. However, once a particular grid was chosen which yielded a reattachment point in agreement with experiment for one step height and inlet velocity, good results were obtained for other step heights and inlet conditions. The reattachment point was found to be insensitive to inlet velocity and was found to move slightly upstream with low rates of wall mass addition. Both of these results are in good agreement with experimental data.[11,12]

A true reattachment point does not exist when mass addition through the wall is present. However, a pseudoreattachment point was calculated by assuming it to occur where the average velocity was zero between the wall and the near-wall node. A comparison of this "reattachment point" with chemical reaction is made with experimental data from nonreacting flows in Fig. 3. It should be noted that the predicted flow reattachment occurred downstream of the Krall-Sparrow[13] maximum heat-transfer point but upstream of the Phaneuf-Netzer[12] data with 10% wall mass addition.

Typical predicted streamline patterns and temperature distributions are presented in Fig. 4 for plexiglas fuel and air. The dividing streamline is also sketched in the temperature field. The recirculation region was calculated to be fuel rich, and the flame initiated along the shear layer and spread out as it approached the reattachment region. The flame region was located within the developing turbulent boundary layer downstream of the reattachment zone. These observations are in qualitative agreement with experiment.

A comparison of predicted plexiglas fuel regression rates with experiment is presented in Fig. 5. It should be noted that the location of the maximum regression rate obtained experimentally was affected by the inlet air distortion/turbulence intensity. The model predicts a maximum regression rate upstream of the experimental values and slightly upstream of the Krall-Sparrow[13] location for maximum heat transfer in nonreacting flow. The average fuel regression rate was in good agreement with experiment, and the regression pattern was qualitatively correct (although shifted upstream). In the present model, only convective transfer to the fuel surface is considered. The predicted regression profile may not be correct for fuel systems that produce large amounts of radiative heat transfer to the surface.

Figure 6 compares the predicted centerline turbulence intensity (assuming isotropic turbulence) with experimental data for nonreacting flow. The behavior with axial distance was generally in good agreement, but the inlet region exhibited behavior not observed experimentally. The model overestimates the velocity increase of the air as it enters the combustor, which in turn reduces the predicted turbulence intensity.

Figure 7 compares experimental and predicted axial pressure profiles. The experiment and theory were not for identical conditions, but in general it is seen that the model predicts the pressure to level off upstream from experimental measurements. This was expected, since the model underestimated the distance to the reattachment point. Pressure calculations were very sensitive to solution accuracy, since they depend upon second derivatives of streamfunction.

Figure 8 presents predicted radial temperature profiles as a function of inlet step size and airflow rate at a location downstream of flow reattachment. As the airflow rate was reduced for a fixed step size, the peak temperature moved

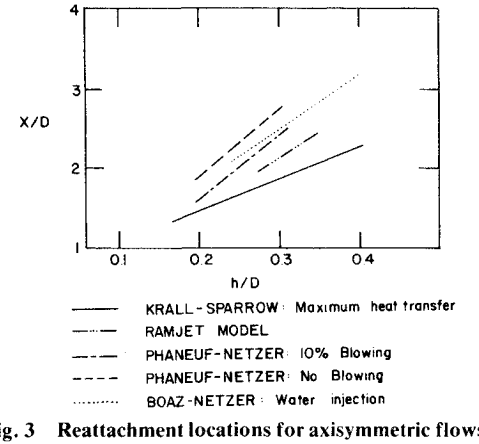

Fig. 3 Reattachment locations for axisymmetric flows.

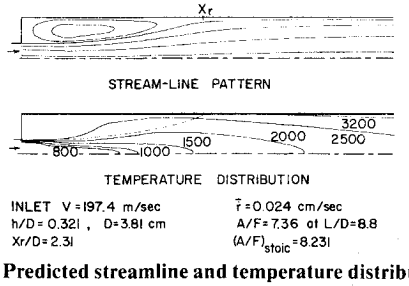

Fig. 4 Predicted streamline and temperature distributions.

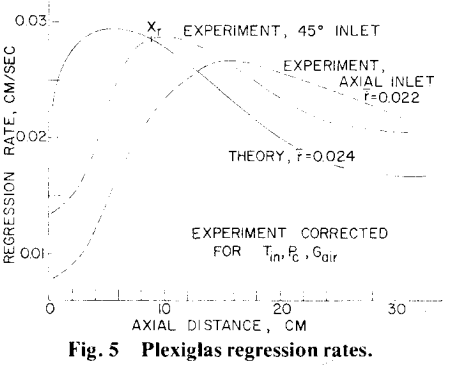

Fig. 5 Plexiglas regression rates.

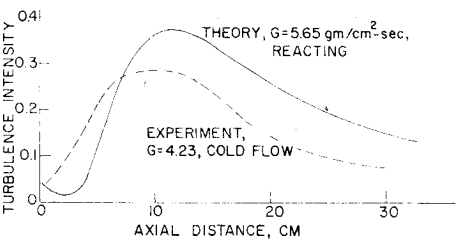

Fig. 6 Centerline turbulence intensity.

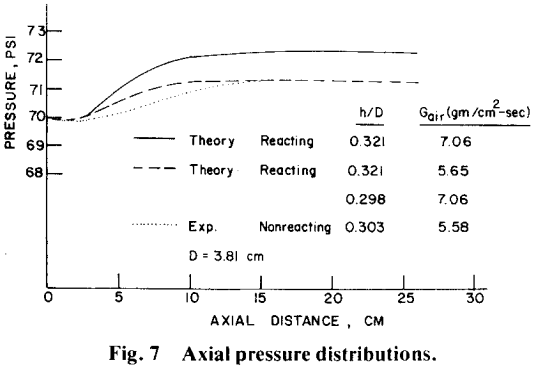

Fig. 7 Axial pressure distributions.

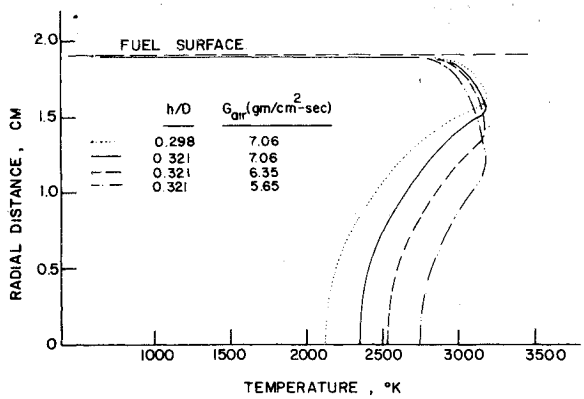

Fig. 8 Predicted radial temperature distributions.

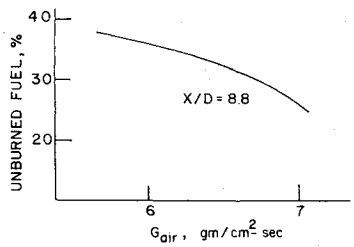

Fig. 9 Predicted fraction of unburned fuel at grain exit.

further from the wall, the core flow became hotter, and the overall fuel-air ratio increased. This results from the fact that regression rate varies as the 0.3 to 0.5 power of G_{air}. Actually the model predicted that $\dot{r} \sim G_{air}^{0.3}$, whereas experimentally it was found for plexiglas that $\dot{r} \sim G_{air}^{0.4}$.

The recirculation zone in the solid-fuel ramjet acts as the flame-stabilization device. It operates fuel rich but, when operating within certain limits, provides enough energy to heat the air in the shear layer to the point where the downstream boundary-layer flame can be stabilized in the high-velocity flow. As the inlet flow rate was increased, the temperature in the upstream portion of the recirculation zone was found to increase. This resulted from the increased air flux into the fuel-rich portion of the zone. However, this same increased air flux into the recirculation zone decreased the temperature in the downstream portion of the zone and at the reattachment position. Thus, although the peak temperatures in the recirculation zone increased with increased inlet air velocity, the oxygen reaching the downstream flame zone decreased in temperature. In addition, the boundary-layer flame narrows and moves closer to the wall. Eventually a condition would be reached where the oxygen reaching the boundary-layer flame region would be too low in temperature to sustain the narrowed flame that exists in the relatively high-velocity region close to the fuel surface. Earlier work with the model,[2,14] in which one-step finite rate kinetics were employed, also demonstrated that increased inlet velocity can cause flame blowoff in either the recirculation region or the boundary-layer region.

Decreasing the inlet step size decreased the length of the shear layer (reattachment occurred further upstream) and decreased the air entrainment into the recirculation region. Although the shear layer was shorter in length, contact time with the recirculation zone did not necessarily decrease because the inlet velocity was lower. However, the model predictions showed a decreased temperature in the recirculation zone, resulting from a still more fuel-rich mixture, and lower temperatures near reattachment. Again it would be expected that a flammability limit would be reached with increasing inlet diameter.

Figure 9 presents the calculated percentage of unburned fuel as a function of airflow rates. As discussed previously, the fuel mass fraction was the least accurate calculation. Thus, the results can only be interpreted qualitatively. As G_{air} is decreased, an increasing amount of unreacted and hotter fuel is passed into the aft mixing region downstream from the end of the fuel grain.

Conclusions and Current Work

The computer model appears to be a good qualitative model for the solid-fuel ramjet combustor. It has several weaknesses (no radiation effects on fuel regression rate, simple kinetics, ψ-ω variables, etc.), but it can be used to qualitatively examine the effects of changes in combustor geometry and test environment. The ψ-ω variables make it difficult to obtain accurate predictions of the pressure field and to specify boundary conditions on the walls. The point iterative method employed also requires large storage space and long computation times.

Current work with the model includes 1) comparison of the model predictions with experimental data obtained in a reacting SFRJ that used an all-hydrocarbon fuel, and 2) extending its application to include the aft-mixing geometry, as shown in Fig. 1. In addition, solutions for the SFRJ geometry are also being investigated using the primary variables of pressure and velocity.

Acknowledgment

This work was sponsored by the Naval Weapons Center, China Lake, Calif.

References

[1] Jensen, G.E., Dunlap, R., and Holzman, A.L., "Solid Fuel Ramjet Flame Stabilization and Fuel Regression Studies," *12th JANNAF Combustion Meeting,* Chemical Propulsion Information Agency 273, Vol. II, Dec. 1975, pp. 425-439.

[2] Netzer, D.W., "Modeling Solid Fuel Ramjet Combustion," *12th JANNAF Combustion Meeting,* CPIA 273, Vol. II, Dec. 1975, pp. 441-450.

[3] Gosman, A.D., Pun, W.M., Runchal, A.K., Spalding, D.B., and Wolfshtein, M., *Heat and Mass Transfer in Recirculating Flows,* Academic Press, New York, 1969.

[4] Spalding, D.B., Gosman, A.D., and Pun, W.M., "The Prediction of Two-Dimensional Flows," short course, Pennsylvania State Univ., Aug. 1973.

[5] Launder, B.E. and Spalding, D.B., *Lectures in Mathematical Models of Turbulence,* Academic Press, New York, 1972.

[6] Jones, W.P. and Launder, B.E., "The Prediction of Laminarization with a Two-Equation Model of Turbulence," *International Journal of Heat and Mass Transfer,* Vol. 15, Feb. 1972, pp. 301-314.

[7] Kaul, U.K. and Frost, W., "Turbulent Atmospheric Flow over a Backward Facing Step," NASA CR-2749, Oct. 1976.

[8] Anasoulis, R.F. and McDonald, H., "A Study of Combustor Flow Computations and Comparison with Experiment," Environmental Protection Agency, EPA-650/2-73-045, Dec. 1973.

[9] Marxman, G.A. and Gilbert, M., "Turbulent Boundary Layer Combustion in the Hybrid Rocket," *Ninth Symposium (International) on Combustion,* Academic Press, New York, 1963, p. 371.

[10] Launder, B.E. and Spalding, D.B., "The Numerical Computation of Turbulent Flows," *Computational Methods in Applied Mechanics and Engineering,* Vol. 3, March 1974, pp. 269-289.

[11] Boaz, L.D. and Netzer, D.W., "An Investigation of the Internal Ballistics of Solid Fuel Ramjets," Naval Postgraduate School, Rept. NPS-57Nt73031A, March 1973.

[12] Phaneuf, J.T. Jr. and Netzer, D.W., "Flow Characteristics in Solid Fuel Ramjets," Naval Postgraduate School, Rept. NPS-57Nt74081, July 1974.

[13] Krall, K.M. and Sparrow, E.M., "Turbulent Heat Transfer in the Separated, Reattached, and Redevelopment Regions of a Circular Tube," *Journal of Heat Transfer,* Vol. 8, Feb. 1966, p. 131.

[14] Jones, C.E. III, Phaneuf, J.T., and Netzer, D.W., "An Investigation of the Internal Ballistics of Solid Fuel Ramjets," *11th JANNAF Combustion Meeting,* CPIA 261, Vol. II, Dec. 1974, pp. 449-470.